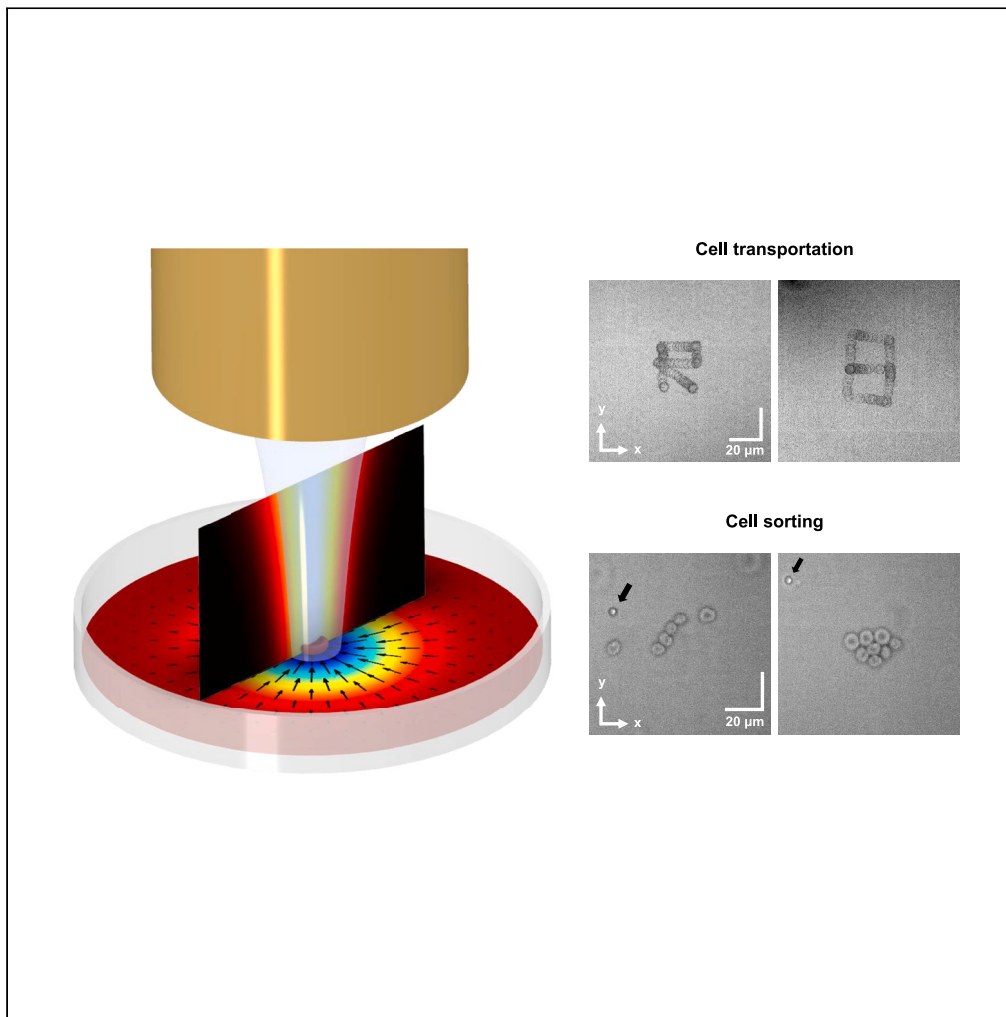


Article

Red blood cell trapping using single-beam acoustic tweezers in the Rayleigh regime



Jinhee Yoo,
Jinhyuk Kim,
Jungwoo Lee,
Hyung Ham Kim

jwlee@kw.ac.kr (J.L.)
david.kim@postech.ac.kr
(H.H.K.)

Highlights

Non-spherical cells are manipulated in a non-invasive and non-contact manner

Cell shape modeling is used to understand trapping dynamics

Acoustic tweezers can be used for *in vivo* cell manipulation

Yoo et al., iScience 26, 108178
November 17, 2023 © 2023 The Author(s).
<https://doi.org/10.1016/j.isci.2023.108178>

Article

Red blood cell trapping using single-beam acoustic tweezers in the Rayleigh regime

Jinhee Yoo,¹ Jinhyuk Kim,² Jungwoo Lee,^{2,*} and Hyung Ham Kim^{1,3,4,5,*}

SUMMARY

Acoustic tweezers (ATs) are a promising technology that can trap and manipulate microparticles or cells with the focused ultrasound beam without physical contact. Unlike optical tweezers, ATs may be used for *in vivo* studies because they can manipulate cells through tissues. However, in previous non-invasive microparticle trapping studies, ATs could only trap spherical particles, such as beads. Here, we present a theoretical analysis of how the acoustic beam traps red blood cells (RBCs) with experimental demonstration. The proposed modeling shows that the trapping of a non-spherical, biconcave-shaped RBC could be successfully done by single-beam acoustic tweezers (SBATs). We demonstrate this by trapping RBCs using SBATs in the Rayleigh regime, where the cell size is smaller than the wavelength of the beam. Suggested SBAT is a promising tool for cell transportation and sorting.

INTRODUCTION

Red blood cells (RBCs) account for 45% of the total blood volume and are essential in supplying oxygen to the body.¹ Hence, RBC disorders, such as anemia and hemoglobinopathy, cause severe health problems. In sickle cell disease, RBCs form a "C" shape and their Young's modulus increases.² Hereditary spherocytosis causes RBCs to become spherical and increases their internal viscosity.³ Moreover, some diseases can affect the physical properties of RBCs. Diabetes and hypercholesterolemia lower the deformability of RBCs and make them coarser.^{4,5} Consequently, the biophysical analysis of RBCs plays a vital role in understanding the link between diseases and hematology, leading to investigating techniques for manipulating single RBCs.

Optical tweezers are suitable for manipulating microparticles and cells such as RBCs.^{6–8} Their invention was awarded the Nobel Prize for enabling biophysical research at the cellular and molecular levels. Recently, acoustic tweezers (ATs) have been used to manipulate cells. Compared to optical tweezers, ATs have a stronger trapping force, can trap larger particles, and have a more comprehensive range of applications from the cellular to the system level.⁹ ATs can also minimize thermal effects on cells by manipulating them within seconds using short pulses. Particularly, by carefully adjusting the acoustic pressure, pulse width, and exposure time, it is possible not to affect the viability of cells.¹⁰ Microscale applications of ATs, such as transportation for moving target cells to the desired position,^{11–14} patterning to create regular shapes,^{11,15,16} and sorting to separate only selected materials or cells,^{17–20} have been studied. In addition, research on the *in vivo* and *ex vivo* manipulation of microparticles has been conducted.^{21–23}

ATs operationalize several principles, such as standing waves, vortices, and single beams.²⁴ Among these, vortex tweezers are the most commonly used principle for non-invasive trapping. In animal studies, microparticles are manipulated by trapping them in blood vessels or the bladder.^{21,22} Another research project, although not involving animals, successfully manipulated microparticles to pass through the human skull.²³ While these studies showed the ability of ATs to perform non-invasive trapping in deep areas, they need a complex system with a multi-element array transducer. Different phase pulses need to be applied to each element for potential well creation, requiring equipment to synchronize the timing. Furthermore, they are limited in being capable of trapping spherical beads rather than non-spherical shapes, such as cells.^{21–23} The challenges in non-invasively trapping cells in deep regions can be attributed to: 1) the limited understanding of shape-dependent nonlinearity, 2) the small size of cells relative to the wavelength, and 3) the impedance of cells, which is not significantly different from the surrounding environment when compared to beads.²² However, living organisms primarily consist of non-spherical particles; therefore, this limitation must be addressed.⁹

Single-beam acoustic tweezers (SBATs) are another non-invasive solution used in single-cell studies without viability issues.^{25–27} SBATs enable precise manipulation without affecting cells, using a short-pulsed high-frequency beam. This is advantageous for cell trapping as it

¹School of Interdisciplinary Bioscience and Bioengineering, Pohang University of Science and Technology (POSTECH), 77 Cheongam-ro, Nam-gu, Pohang-si, Gyeongbuk 37673, Republic of Korea

²Department of Electronic Engineering, Kwangju University, Seoul 01897, Republic of Korea

³Department of Convergence IT Engineering, Pohang University of Science and Technology (POSTECH), 77 Cheongam-ro, Nam-gu, Pohang-si, Gyeongbuk 37673, Republic of Korea

⁴Department of Electrical Engineering, Pohang University of Science and Technology (POSTECH), 77 Cheongam-ro, Nam-gu, Pohang-si, Gyeongbuk 37673, Republic of Korea

⁵Lead contact

*Correspondence: jwlee@kw.ac.kr (J.L.), david.kim@postech.ac.kr (H.H.K.)

<https://doi.org/10.1016/j.isci.2023.108178>



utilizes wavelengths similar to the size scale of cells. Additionally, high frequencies enable strong interactions at boundaries with similar impedance, allowing effective force application on cells.^{28,29} In addition, due to the use of a single element, the system is simple, and intense ultrasound is applied at a single point, leading to strong trapping force and stable trapping capabilities.³⁰ There are two SBAT types: the Mie and Rayleigh regimes. SBATs in the Mie regime operate when the wavelength is less than the object's size.^{31,32} Because the cell size is on the micrometer scale, high frequencies (above 20 MHz) and high focus (f-number less than 2) are required. Therefore, they are suitable for *in vitro* studies and have been used to measure the physical and biological properties of a single particle.^{27,33–35} SBATs in the Rayleigh regime work when the wavelength is greater than the object's size.^{29,32} They work even with longer focal depths and wider beam widths than those in the Mie regime. Unlike the Mie regime, the Rayleigh regime has not yet been widely used in various applications and has primarily been investigated through numerical studies.^{29,30} Therefore, SBATs in the Rayleigh regime have a greater potential for non-invasive trapping of cells in deep regions compared to other types of tweezers, but there is still a lack of theoretical studies, particularly regarding non-spherical objects.

In this study, we addressed the limitations of previous research on non-invasive ATs in their ability to trap cells in deep regions.^{21–23} We demonstrated a solution by trapping RBCs with SBATs in the Rayleigh regime. Compared to conventional non-invasive ATs, SBATs in the Rayleigh regime are better suited for cell trapping using high frequencies and offer a simpler system structure with a single-element configuration.^{25,26} However, studies regarding non-spherical cells are still limited. To address this problem, we conducted numerical analysis based on the biconcave modeling of RBCs. In contrast to previous studies that did not consider shape modeling, we were able to elucidate the discrepancy in trapping potential and trapping force between RBCs and polystyrene (PS) beads of similar size. We compared the calculated trapping force for these two particles with experimental results from two aspects: dynamics with respect to lateral distance from the focal point and dynamics to travel distance. Our analysis covered a greater number of parameters compared to previous numerical studies on SBATs in the Rayleigh regime and demonstrated consistency with experimental results. Therefore, this study contributes to a more concrete theoretical understanding of SBATs in the Rayleigh regime and analyzes the non-invasive trapping dynamics of non-spherical cells based on their contours for the first time.

The proposed tweezers were applied in two practical applications: cell transportation and sorting. Although the ultrasound gel pad was in the acoustic path, PS beads and RBCs were stably manipulated at the desired coordinate point. This could trap without noise, such as rotation, which was observed in vortex tweezers studies.^{22,36} Furthermore, while previous studies on SBATs in the Rayleigh regime have provided trapping capabilities based on the size of the particles,^{29,32} the proposed tweezers could sort objects of similar size depending on the materials properties. From these applications, there is great potential for various studies related to RBCs. The proposed ATs can measure the deformability and elasticity of RBCs by trapping and exerting forces on them.³⁴ By measuring inter-forces between RBCs and various cells or substances using the trapping force of RBC, the membrane mechanics of RBCs can be understood.^{37,38} In addition, manipulation of cells in the vasculature can contribute to hemodynamics research and the development of *in vivo* flow cytometry.³⁹ We anticipate that this study will have significant implications for both biophysics and biomedical engineering.

RESULTS AND DISCUSSION

Calculation of trapping force using an approximate RBC model

The SBATs in the Rayleigh regime can produce a potential well by using a single-element tweezer only (Figure 1A).²⁹ Previous numerical studies based on spherical models could not analyze the dynamics of RBC trapping because they did not consider the complex contours of RBCs. Therefore, the phenomenon of RBC becoming trapped in the focal depth while PS beads of similar size were not trapped was difficult to explain. To address this, we employed biconcave modeling of the RBC (Figure 1B). An RBC was placed parallel to the XY-plane, with its analytical expression $S(x, y, z)$ given by Equation 1, where the RBC radius is r which is $4 \mu\text{m}$ in this case. Note that the values of A , B , and C were set to 0.207161, 2.002558, and -1.122762 , respectively.⁴⁰

$$S(x, y, z) = 0.5r\sqrt{1 - \frac{(x^2+y^2)}{r^2}} \left\{ A + B \frac{(x^2+y^2)}{r^2} + C \frac{(x^2+y^2)^2}{r^4} \right\} \pm z = 0 \quad (\text{Equation 1})$$

$$R = \frac{\left\{ 1 + \left(\frac{dy}{dx} \right)^2 \right\}^{3/2}}{\left| \frac{d^2y}{dx^2} \right|} \quad (\text{Equation 2})$$

Next, an approximation was made, as shown in Figure 1C. A point $P(x_0, y_0, z_0)$ on the biconcave surface was considered to be one on an imaginary sphere with a tangential plane identical to that of the RBC at the same point. Consequently, the equivalent sphere has a center at point $C(x_c, y_c, z_c)$ located along line CP , and the normal vector to the plane is represented by Equation 3.

$$\nabla S(x_0, y_0, z_0) = (n_x, n_y, n_z) = \vec{n} \quad (\text{Equation 3})$$

Therefore, point C is determined as follows:

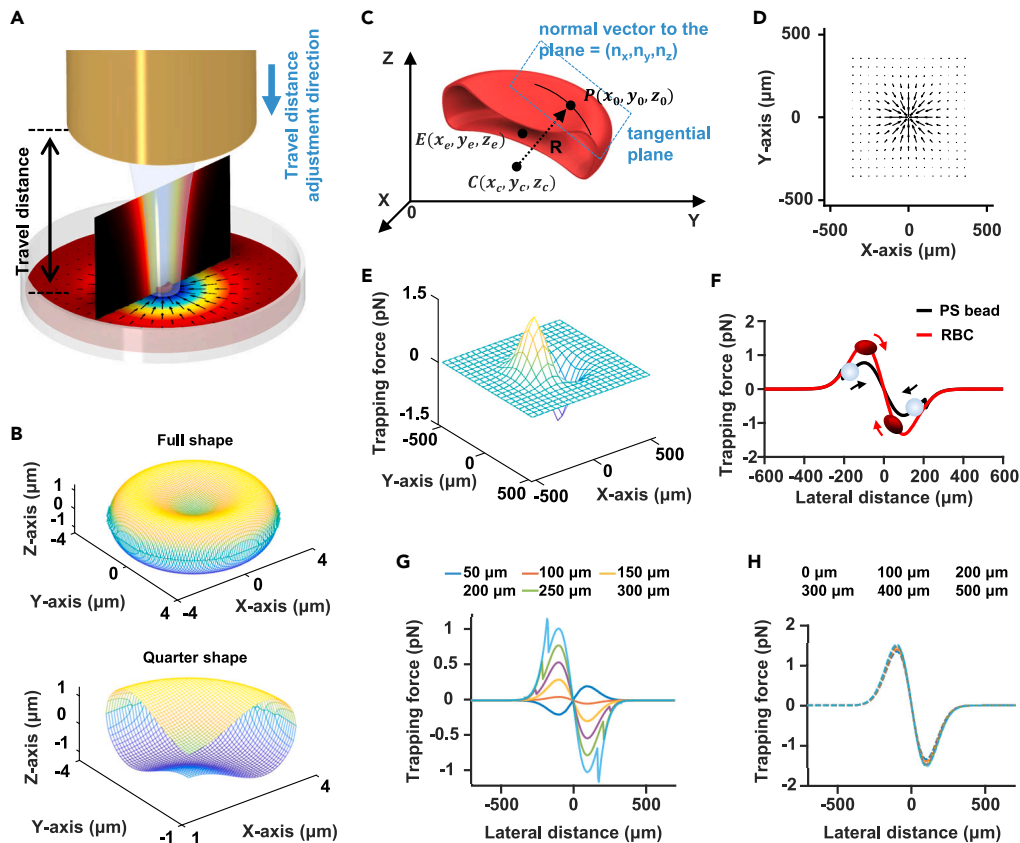


Figure 1. RBC trapping using SBATs in the Rayleigh regime

(A) Configuration of ATs in which the RBC is trapped. The sub-wavelength RBC is trapped by a Gaussian-distributed beam of single-element ATs. The travel distance was adjusted only in the direction closer to the bottom surface.

(B) Full and quarter modeling shape of the RBC.

(C) The coordinate system of the RBC model for force computation. E, center of the RBC; C, center of the imaginary sphere; P, a point on the surface of the RBC; R, the radius of curvature.

(D) The trapping force of RBCs in 2D. The RBC was calculated to be trappable at the focal depth.

(E) The trapping force of RBCs in the x-direction in 2D.

(F) The trapping force on the PS beads and RBCs. The force is expressed in the transverse direction (x axis).

(G) The trapping force on the PS bead depends on travel distance.

(H) The trapping force on the RBC depends on the travel distance.

The legend in Figures G and H represents how much the travel distance is shorter compared to the focal depth (0 μm means focal depth). The acoustic power for the calculations in each figure is assumed to be 3 mW.

$$\vec{OC} = \vec{OP} + \frac{R}{|\vec{n}|^2} \vec{n} + \vec{OE} \quad (\text{Equation 4})$$

By measuring the force of the imaginary sphere, we calculated the trapping force from the biconcave shape of the RBC (Figure 1D). The trapping force pattern matched the Gaussian acoustic pressure distribution (Figure S1), indicating that a potential well was formed around the focal point. To visualize the value of the trapping force at each coordinate, we obtained the trapping force of the x-direction component (Figure 1E). In addition, the transverse trapping force of the RBC was obtained from the data when $y = 0$ in the trapping force of the x-direction component (Figure 1F). Because the two-dimensional trapping force was symmetrical at the origin, the trapping patterns could be analyzed depending on the conditions with only one-dimensional results. For the PS beads, the distance between the tweezer and the particle was assumed to be 250 μm less than the focal depth. For the RBC, the distance was assumed to be equal to the focal depth.

In SBATs in the Rayleigh regime, particles may or may not be trapped by varying the trapping force depending on various conditions, such as the travel distances and the sizes of the microparticles.^{29,32} Travel distance is defined by the distance from the tweezer's surface to the microparticles, where ultrasound is transmitted (Figure 1A). In this study, the travel distance was adjusted by moving the tweezer toward the substrate, exploring how much the height was lowered relative to the focal depth. Firstly, we evaluated the impact of travel distance on trapping efficiency for a 5- μm PS bead through numerical analysis. If the travel distance was the focal depth of the tweezers, no trapping

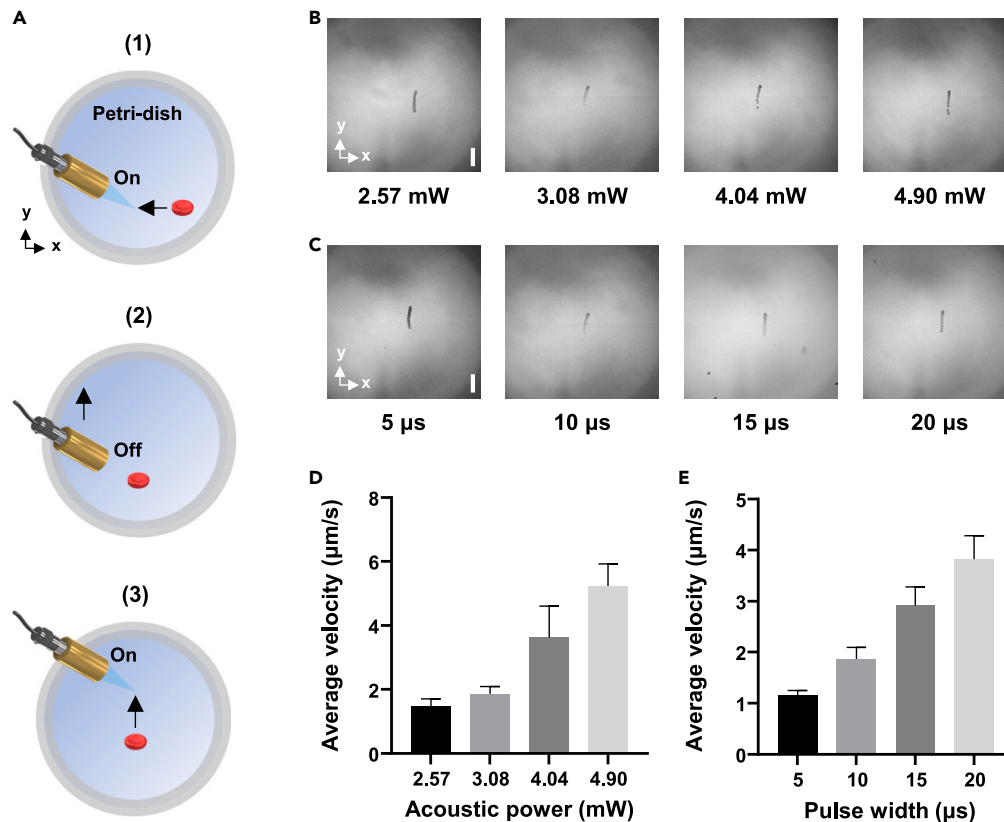


Figure 2. Experimental results for the RBC trapping conditions

(A) The sequence of the trapping force evaluation experiment. (1) A free single RBC was trapped in the focal point. (2) When the RBC reached the focal point, the tweezers were turned off and moved to the desired position. This position corresponded to the distance that we wanted to move the RBC. (3) The tweezer was switched on, and the movement of the RBC was observed.

(B) mIP image depending on acoustic power.

(C) mIP image depending on pulse width. In Figures 2B and 2C, the averaged velocity was obtained when particles moved approx. 45 μm .

(D) Average speed depends on acoustic power. The pulse width was fixed at 10 μs .

(E) Average speed depends on pulse width. Acoustic power was set to 3.08 mW.

In Figures 2D and 2E, representative of $n = 3$. The graph represents the mean \pm SD. Scale bars in B and C: 40 μm .

occurred, even at 50 μm less than the focal depth (Figures 1G and S2A). However, the PS beads were trapped well within 100 μm , which is less than the focal depth. In addition, the less the travel distance, the stronger the trapping force (Figures 1G and S2B). The RBCs were well trapped at the focal depth, and there was no significant change in the trapping force, even when the travel distance was reduced (Figure 1H). This is related to the acoustic impedance of the trapped particles. The acoustic impedances of the water, PS beads, and RBCs were 1.5, 2.5, and 1.8 MRays, respectively. The PS beads generated more reflections owing to the significant difference in acoustic impedance with water, which had complex acoustic energy due to reverberation inside and outside the sphere.⁴¹ Meanwhile, the RBCs responded to acoustic energy without experiencing multiple reflections. To support this explanation, we calculated the trapping force by assuming an artificial bead with an impedance similar to that of an RBC and found it trapped well (Figure S2F). Furthermore, the low impedance of the cell may adversely affect trapping because acoustic energy minimally affects trapping.^{41,42} In this case, a sufficiently high frequency was required, and in this study, a frequency of 30 MHz was sufficient for cell trapping.

Trapping conditions

The trapping force is determined by the acoustic waves propagating from the AT. The trapping force was evaluated to demonstrate this by obtaining the average velocity of the particles moving approximately 45 μm (Figure 2A). We applied 11.22, 12.21, 13.86, and 15.18 V_{pp} to the tweezers, corresponding to acoustic pressures of 0.27, 0.30, 0.34, and 0.38 MPa, and acoustic powers of 2.57, 3.08, 4.04, and 4.90 mW, respectively (Figure S1B). The acoustic pressure was measured using a hydrophone, and the acoustic intensity was calculated by dividing the square of the pressure by the impedance. The power was computed by multiplying the area of the beam profile (Figures S1C and S1F). The results indicate that the stronger the output acoustic power, the faster the movement of the microparticles (Figures 2B and 2D). The movement of RBCs was visualized using minimum-intensity projection (mIP) images. The mIP images were obtained from the recorded video stacks to

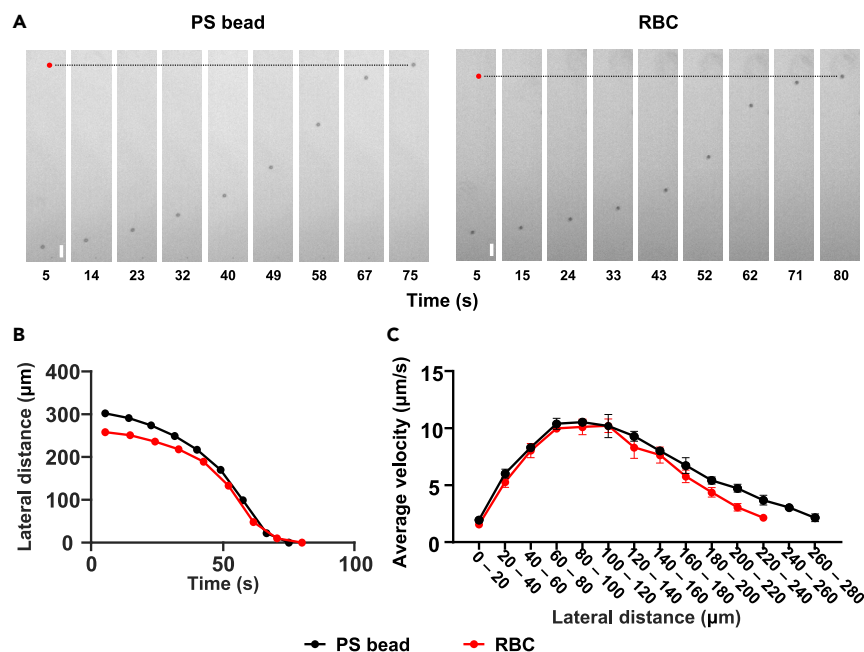


Figure 3. Measuring the average velocity of trapped single PS bead and RBC

(A) Changing the position of the trapped PS bead and RBC over time. The photos are equally divided into nine segments from the start of trapping until the focal point is reached. The red dots are the focal points.

(B) Time-dependent movement of microparticles in Figure 3A from the focal point.

(C) The average velocity of a trapped PS bead and RBC. The change of position in average velocity was calculated at intervals of approximately 20 μm , depending on the distance from the focal point.

Representative of $n = 3$. The graph represents the mean \pm SD. Scale bars: 20 μm .

visualize movement over time. This is because a higher acoustic power produces a deeper potential well and has a stronger trapping force. Even when the pulse width increased, the movement of particles was faster (Figures 2C and 2E). The trapping force increased because increasing the pulse width increased the acoustic energy at the same power.⁴³ The SBAT using the parameters employed in this study does not affect the viability of RBCs (Figure S3).

Based on these results, the appropriate acoustic power and pulse width were determined. For example, to observe the movement of microparticles in detail, even at a low frame rate, the experiment was conducted with an acoustic power of 3.08 mW and a pulse width of 10 μs . These conditions were sufficient to trap microparticles and allowed them to move slowly, offering detailed observations of their motion. Although smaller power and pulse width could be employed, they may not ensure a stable trap. To determine the trapping performance, the pulse width was increased to 20 μs . This condition provided more stable trapping than the condition at lower pulse widths. Increasing the acoustic power was one method; however, the pulse width was first increased because it could be affected nonlinearly when the microparticles were bulked. In this study, due to the use of appropriate acoustic parameters, we did not observe any cell deformation.

Average velocity analysis

The numerical analysis of the calculated trapping dynamics was compared and verified with experimental results. PS beads and RBCs were trapped with an acoustic power of 3.08 mW and pulse width of 10 μs , in the same way as in Figures 2A, 3A, and 3B. The PS bead and RBC were recorded for a total duration of 75 and 80 s, respectively (Figure 3B). While relocating the tweezers, the position of the microparticle remained unstable for approximately 5 s, and this portion of the data was not used to analyze. The total video was divided into nine sequential images, excluding this tweezer repositioning time, and visualized with the corresponding time indicated (Figure 3A). When trying to trap microparticles over a certain distance, they were loosely trapped or not trapped. To prevent this error, the maximum trapping distance was determined to be the distance of three consecutive successful trappings. The maximum trapping distances of the PS beads and RBC were set to 300 and 260 μm , respectively (Figures 3 and S4). In this experiment, measuring the short duration of the microparticle's movement caused errors in the measurement owing to problems such as trapping vibration and low camera frame rate. To solve this problem, the section was analyzed by dividing it by 20 μm , which is a length that can sufficiently measure the average speed.

The experiment results indicated that both microparticles attained maximum velocity in the 80–100 μm section, and the velocity rapidly decreased as they approached the focal point (Figure 3C, Videos S1 and S2). This is consistent with the numerical calculation, which shows the maximum trapping force at the lateral distance of 100 μm in Figure 1F. This is because the acceleration is greatest when the microparticles experience the greatest force, and the average speed is greatest in the section where the acceleration is the greatest. In addition, the

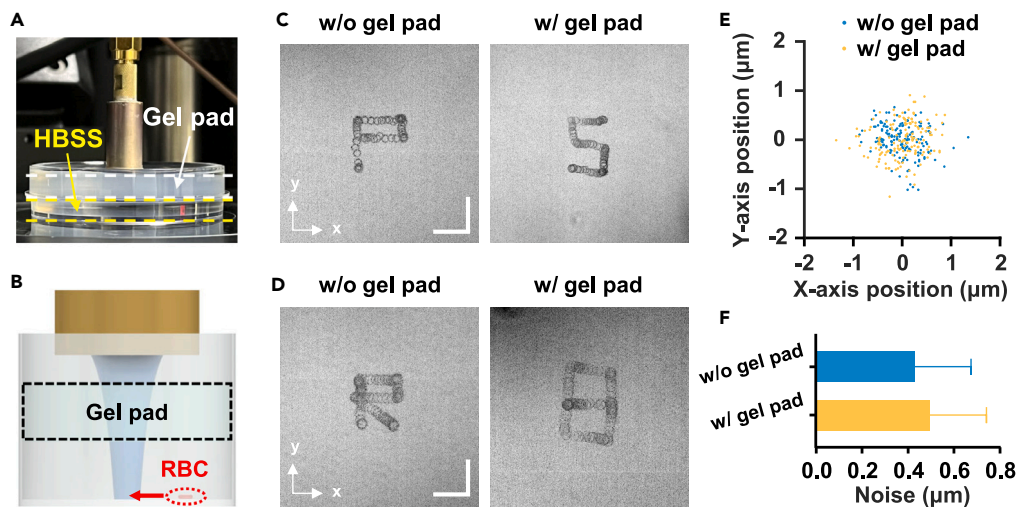


Figure 4. Single PS bead and RBC trapping

(A) Photo of microparticle trapping with a gel pad.
 (B) Schematic diagram of microparticle trapping with a gel pad.
 (C) mIP images of a trapped PS bead.
 (D) mIP images of a trapped RBC.
 (E) Observe the movement of RBCs trapped in one position.
 (F) Noise for trapped RBCs with and without gel pads.

One set of data consists of 50 data points obtained at 0.2 s intervals for 10 s, and each condition is represented by three sets. Bar graphs represent mean \pm SD. Scale bars in C and D: 20 μm .

maximum force on the RBCs was approximately 1.7 times the maximum force on the PS beads. Still, their average velocities were similar because the acceleration was similar, but the weights differed. The volume of a single RBC obtained through RBC modeling used in this study was approximately 100 μm^3 , which is a typical value.⁴⁴ Because the PS beads were spherical, their volume could be obtained easily. By multiplying the density of each particle, the masses of the RBC and PS beads were calculated to be 0.11 and 0.07 ng, respectively. The mass of RBC was approximately 1.6 times the mass of the PS beads, which can explain the similarity of the average velocities of the two particles in the simulation results in Figure 1F.

PS bead and RBC transportation

Cell transportation has been studied in various fields, such as nanotechnology and biomedicine, using microrobots, optics, and acoustics.^{8,45} We investigated the feasibility of applying SBATs in the Rayleigh regime for non-contact particle transport applications. After trapping the microparticles, the position of the tweezer was changed to ensure that they were accurately and stably trapped. PS beads and RBCs were trapped with an acoustic power of 3.08 mW and a pulse width of 20 μs . In addition, this experiment demonstrated the possibility of non-invasive trapping by adding an ultrasound gel pad (Bluemtech, Gangwon-do, Korea) to the acoustic pathway (Figures 4A and 4B). A 7-mm-thick gel pad was placed in a Petri dish filled with Hanks' balanced salt solution, and the results were analyzed with and without gel pads.

A single PS bead and an RBC were manipulated into the shapes of letters "P" and "R," respectively (Figures 4C and 4D, and Video S3). Images were visualized as mIP images. These results demonstrate that SBATs in the Rayleigh regime have sufficient force and stability to trap PS beads and RBCs. Subsequently, microparticles were manipulated by placing a gel pad on the acoustic path. A single PS bead and an RBC were manipulated into the shape of letters "S" and "B," respectively (Figures 4C and 4D, and Video S3). Although these results were not as accurate as those obtained without a gel pad, they showed that non-contact and non-invasive manipulation of microparticles was possible.

Moreover, we quantitatively compared the accuracy obtained with and without the gel pad by measuring noise (Figure 4E, F). The trapping point of RBC was monitored for small movements at 0.2-s intervals for 10 s, with each condition being repeated three times. The noise was measured as the distance from the focal point to the RBC, and measurements were performed for three cells for each condition. The noise was approximately 0.4 μm , indicating stable trapping considering the micron-level cell size and movement. Although the gel pad had a statistically significant effect (two-tailed t test assuming equal variance, $p = 0.02$), the difference in the results was slight, approximately 0.06 μm (Figure 4F).

These results demonstrate that SBATs in the Rayleigh regime have a high potential for application in cell transportation. In this study, a single RBC was manipulated at a distance of 12.65 mm through a 7-mm-thick gel pad. In addition, it was manipulated at the exact coordinates of a point. Because the Gaussian radial distribution of acoustic pressure was used, it was temporally stable (noise less than 1 μm). In contrast, vortex tweezers can generate torque, which may cause noise when observing motion.^{22,36} We expect this research will be helpful for *in vivo* or *in vitro* single-cell studies requiring high precision.

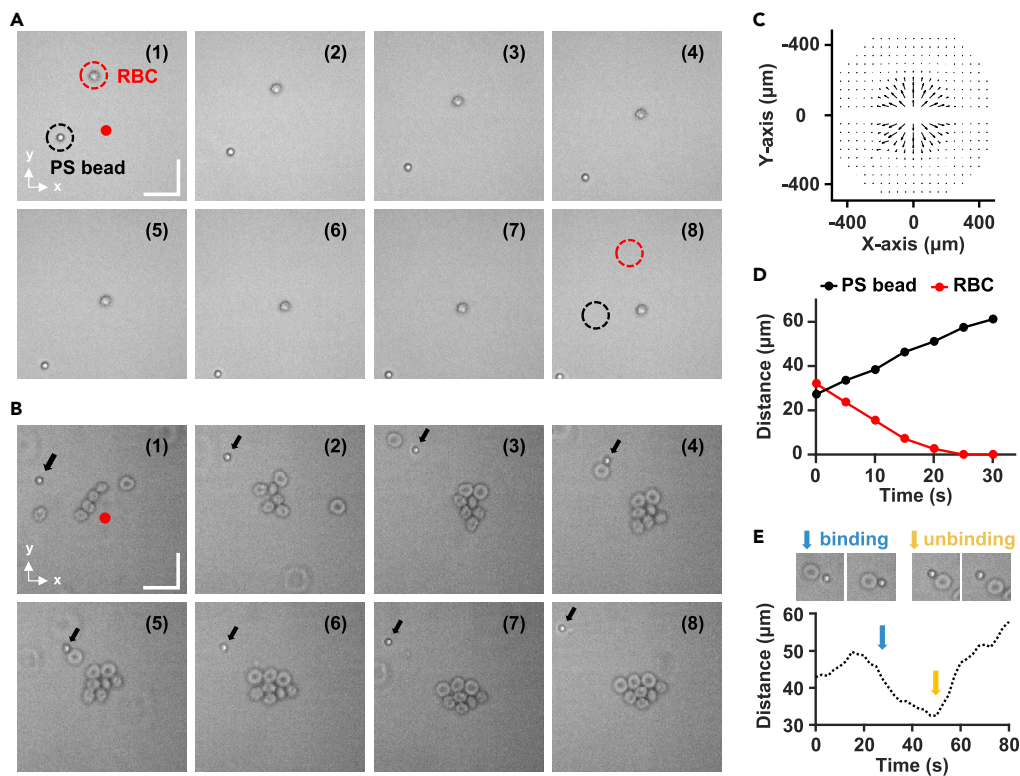


Figure 5. Cell sorting based on travel distance

(A) Separation of a single RBC. The red dot is the focal point, the red dotted circle is the original position of the RBC, and the black dotted circle is the original position of the PS bead.

(B) Separation of multiple RBCs. The red dot is the focal point, and the black arrow is the position of the PS bead.

(C) The trapping force of the PS bead in 2D. The PS bead was calculated to be non-trappable at depths below 50 μm from the focal depth. The acoustic power was assumed to be 3 mW.

(D) Time-dependent movement of a PS bead and RBC from the focal point in Figure 5A.

(E) Time-dependent movement of a PS bead from the focal point in Figure 5B. The blue arrow is the point where a PS bead and RBC start to bind, and the yellow arrow is the point where they unbind.

Scale bars in A and B: 20 μm .

Cell sorting based on the travel distance

Cell sorting is widely used in various fields, such as cell biology and biomedical research. Several label-free sorting methods have been studied, including optical, magnetic, and acoustic approaches.^{46,47} We present the SBATs in the Rayleigh regime as another label-free sorting method. Because this experiment assumes a non-invasive situation, it cannot be sorted spatially but can be divided into focus and out-of-focus. We demonstrated that depending on the travel distance, the target cell may or may not be trapped, as shown in Figures 1G and 1H. This difference was used to separate the RBCs and beads. To sort individual RBCs and RBC clusters (Figures 5A and 5B, Videos S4 and S5), we applied a focused beam with an acoustic power of 3.08 mW, a pulse width of 10 μs , and an adjusted travel distance of 50 μm below the focal depth. The sorted RBC clusters are also positionally manipulable (Figure S5).

For single RBC sorting (Figure 5A and Video S4), we first placed the RBCs and PS beads at a distance similar to that of the focal point. When the tweezers were switched on, an RBC was trapped at the focal point, but the PS bead moved away. The numerical calculations showed that the PS bead moved away in the radial direction from the focal point when it was trapped (Figure 5C), and the same result was obtained experimentally. Considering the movement of the RBC, we observed that it took 16 s to move 20 μm , and the average movement speed was 1.3 $\mu\text{m}/\text{s}$ (Figure 5D), similar to the previous results shown in Figure 3C.

For multiple RBCs sorting (Figure 5B and Video S5), separate movement of a single PS bead was observed while trapping multiple RBCs (Figure 5E). The distance between the PS bead and the focal point increased at the beginning of the trapping. However, after a few seconds, the PS bead came into contact with the trapped RBC, and they moved together because of some mechanism, such as a hydrophobic interaction.^{48,49} This indicates that the force needed to trap the RBC is stronger than that required to push the PS bead. After approximately 20 s, the PS bead was unbound from the RBC and moved away from the focus again. The unbinding demonstrates that the sum of the forces pushing the PS bead and those trapping the RBCs is greater than the binding force between the PS bead and the RBC. As a result, we observed the

formation of an RBC cluster and the dynamics of interparticle binding forces, which were mainly studied with optical and magnetic tweezers.^{8,49,50}

We can conclude that SBATs in the Rayleigh regime can sort microparticles by type by adjusting the travel distance. We verified the feasibility of cell sorting through simulations (Figures 1G and 1H) and experimentally demonstrated the same results (Figure 5). RBCs were sorted from the beads because they have different travel distances that can be trapped depending on the characteristics of the microparticles. Previous studies sorted particles by size,^{29,32} but in this study, we could sort different particles of similar size. Because the cell sorting method presented in this study is non-invasive, it is expected to be helpful for *in vivo* or microfluidic biophysics as a technique for measuring interparticle binding forces.^{8,49,51}

Limitations of the study

This study has demonstrated the characteristic of non-invasiveness in a deep region. However, it was not possible to experimentally observe this *in vivo* due to the difficulty of observing the dynamics of a single cell in the deep region of an animal model. Previous studies have measured it in a thin flap that could be observed under a microscope or trapped a large bead.^{21,22} Therefore, this study can approach more practical applications with the technology to observe the movement of a single cell in the deep region. Another limitation is the lack of z axis analysis. Since this study was conducted in a Petri dish, analysis of the z axis is not necessary. However, for application in 3D environments such as animal models, analysis of z axis trapping is necessary. Recent research on acoustic levitation or three-dimensional ATs has been studied to complement these points.^{52–54} Through in-depth theoretical and experimental understanding of trapping dynamics along with these studies, we can gain a better understanding of non-invasive trapping for animal studies.

STAR★METHODS

Detailed methods are provided in the online version of this paper and include the following:

- KEY RESOURCES TABLE
- RESOURCE AVAILABILITY
 - Lead contact
 - Materials availability
 - Data and code availability
- EXPERIMENTAL MODEL AND STUDY PARTICIPANT DETAILS
 - Human RBC
- METHOD DETAILS
 - Derivation of acoustic radiation force
 - Single-element acoustic tweezers fabrication
 - Trapping of the PS bead and RBC
 - Imaging setup and data analysis
 - Average velocity calculation
- QUANTIFICATION AND STATISTICAL ANALYSIS

SUPPLEMENTAL INFORMATION

Supplemental information can be found online at <https://doi.org/10.1016/j.isci.2023.108178>.

ACKNOWLEDGMENTS

This research was supported by the Basic Science Research Program through the National Research Foundation of Korea (NRF) funded by the Ministry of Education (2022R1A6A3A13072066 and 2020R1A6A1A03047902) and the Korean government (MSIT) (2022R1A2B5B0200219311), the Research Grant of Kwangwoon University in 2023, and BK21 FOUR.

AUTHOR CONTRIBUTIONS

Conceptualization, J.Y., J.L., and H.H.K.; methodology, J.Y., J.L., and H.H.K.; formal analysis, J.Y., J.K., and J.L.; investigation, J.Y.; writing – original draft, J.Y.; writing – review & editing, J.L. and H.H.K.; supervision, J.L. and H.H.K.; project administration, J.L. and H.H.K.; funding acquisition, J.Y., J.L., and H.H.K.

DECLARATION OF INTERESTS

The authors declare no competing interests.

INCLUSION AND DIVERSITY

We support inclusive, diverse, and equitable conduct of research.

Received: April 4, 2023
Revised: August 2, 2023
Accepted: October 9, 2023
Published: October 11, 2023

REFERENCES

- Mozos, I. (2015). Mechanisms Linking Red Blood Cell Disorders and Cardiovascular Diseases. *BioMed Res. Int.* 2015, 1–12. <https://doi.org/10.1155/2015/682054>.
- Maciaszek, J.L., and Lykotrafitis, G. (2011). Sickle cell trait human erythrocytes are significantly stiffer than normal. *J. Biomech.* 44, 657–661. <https://doi.org/10.1016/j.jbiomech.2010.11.008>.
- Mohandas, N., Clark, M.R., Jacobs, M.S., and Shohet, S.B. (1980). Analysis of factors regulating erythrocyte deformability. *J. Clin. Invest.* 66, 563–573. <https://doi.org/10.1172/JCI109888>.
- Babu, N. (2009). Influence of hypercholesterolemia on deformability and shape parameters of erythrocytes in hyperglycemic subjects. *Clin. Hemorheol. Microcirc.* 41, 169–177. <https://doi.org/10.3233/CH-2009-1165>.
- Li, H., Papageorgiou, D.P., Chang, H.-Y., Lu, L., Yang, J., and Deng, Y. (2018). Synergistic Integration of Laboratory and Numerical Approaches in Studies of the Biomechanics of Diseased Red Blood Cells. *Biosensors* 8, 76. <https://doi.org/10.3390/bios8030076>.
- Ashkin, A., Dziedzic, J.M., Bjorkholm, J.E., and Chu, S. (1986). Observation of a single-beam gradient force optical trap for dielectric particles. *Opt. Lett.* 11, 288. <https://doi.org/10.1364/OL.11.000288>.
- Ashkin, A. (1997). Optical trapping and manipulation of neutral particles using lasers. *Proc. Natl. Acad. Sci. USA* 94, 4853–4860. <https://doi.org/10.1073/pnas.94.10.4853>.
- Zhang, H., and Liu, K.K. (2008). Optical tweezers for single cells. *J. R. Soc. Interface* 5, 671–690. <https://doi.org/10.1098/rsif.2008.0052>.
- Rufo, J., Zhang, P., Zhong, R., Lee, L.P., and Huang, T.J. (2022). A sound approach to advancing healthcare systems: the future of biomedical acoustics. *Nat. Commun.* 13, 3459–3468. <https://doi.org/10.1038/s41467-022-31014-y>.
- Guzmán, H.R., Nguyen, D.X., Khan, S., and Prausnitz, M.R. (2001). Ultrasound-mediated disruption of cell membranes. I. Quantification of molecular uptake and cell viability. *J. Acoust. Soc. Am.* 110, 588–596. <https://doi.org/10.1121/1.1376131>.
- Guo, F., Mao, Z., Chen, Y., Xie, Z., Lata, J.P., Li, P., Ren, L., Liu, J., Yang, J., Dao, M., et al. (2016). Three-dimensional manipulation of single cells using surface acoustic waves. *Proc. Natl. Acad. Sci. USA* 113, 1522–1527. <https://doi.org/10.1073/pnas.1524813113>.
- Yoon, C., Kang, B.J., Lee, C., Kim, H.H., and Shung, K.K. (2014). Multi-particle trapping and manipulation by a high-frequency array transducer. *Appl. Phys. Lett.* 105, 214103. <https://doi.org/10.1063/1.4902923>.
- Li, J., Shen, C., Huang, T.J., and Cummer, S.A. (2021). Acoustic tweezer with complex boundary-free trapping and transport channel controlled by shadow waveguides. *Sci. Adv.* 7, 1–7. <https://doi.org/10.1126/sciadv.abi5502>.
- Guo, F., Zhou, W., Li, P., Mao, Z., Yennawar, N.H., French, J.B., and Huang, T.J. (2015). Precise Manipulation and Patterning of Protein Crystals for Macromolecular Crystallography Using Surface Acoustic Waves. *Small* 11, 2733–2737. <https://doi.org/10.1002/sml.201403262>.
- Collins, D.J., Devendran, C., Ma, Z., Ng, J.W., Neild, A., and Ai, Y. (2016). Acoustic tweezers via sub-time-of-flight regime surface acoustic waves. *Sci. Adv.* 2, e1600089. <https://doi.org/10.1126/sciadv.1600089>.
- Shapiro, J.M., Drinkwater, B.W., Perriman, A.W., and Fraser, M. (2021). Sonolithography: In-Air Ultrasonic Particulate and Droplet Manipulation for Multiscale Surface Patterning. *Adv. Mater. Technol.* 6, 2000689. <https://doi.org/10.1002/admt.202000689>.
- Ding, X., Lin, S.-C.S., Lapsley, M.I., Li, S., Guo, X., Chan, C.Y., Chiang, I.-K., Wang, L., McCoy, J.P., and Huang, T.J. (2012). Standing surface acoustic wave (SSAW) based multichannel cell sorting. *Lab Chip* 12, 4228–4231. <https://doi.org/10.1039/c2lc40751e>.
- Meng, L., Cui, X., Dong, C., Liu, X., Zhou, W., Zhang, W., Wang, X., Niu, L., Li, F., Cai, F., et al. (2020). Microbubble enhanced acoustic tweezers for size-independent cell sorting. *Appl. Phys. Lett.* 116. <https://doi.org/10.1063/1.5123544>.
- Wu, M., Huang, P.H., Zhang, R., Mao, Z., Chen, C., Kemeny, G., Li, P., Lee, A.V., Gyanchandani, R., Armstrong, A.J., et al. (2018). Circulating Tumor Cell Phenotyping via High-Throughput Acoustic Separation. *Small* 14, 1801131. <https://doi.org/10.1002/sml.201801131>.
- Zhong, R., Yang, S., Ugolini, G.S., Naquin, T., Zhang, J., Yang, K., Xia, J., Konry, T., and Huang, T.J. (2021). Acoustofluidic Droplet Sorter Based on Single Phase Focused Transducers. *Small* 17, 2103848. <https://doi.org/10.1002/sml.202103848>.
- Ghanem, M.A., Maxwell, A.D., Wang, Y.-N., Cunitz, B.W., Khokhlova, V.A., Sapozhnikov, O.A., and Bailey, M.R. (2020). Noninvasive acoustic manipulation of objects in a living body. *Proc. Natl. Acad. Sci. USA* 117, 16848–16855. <https://doi.org/10.1073/pnas.2001779117>.
- Lo, W.-C., Fan, C.-H., Ho, Y.-J., Lin, C.-W., and Yeh, C.-K. (2021). Tornado-inspired acoustic vortex tweezer for trapping and manipulating microbubbles. *Proc. Natl. Acad. Sci. USA* 118, e2023188118. <https://doi.org/10.1073/pnas.2023188118>.
- Yang, Y., Ma, T., Li, S., Zhang, Q., Huang, J., Liu, Y., Zhuang, J., Li, Y., Du, X., Niu, L., et al. (2021). Self-Navigated 3D Acoustic Tweezers in Complex Media Based on Time Reversal. *Research* 2021, 9781394. <https://doi.org/10.34133/2021/9781394>.
- Meng, L., Cai, F., Li, F., Zhou, W., Niu, L., and Zheng, H. (2019). Acoustic tweezers. *J. Phys. D Appl. Phys.* 52, 273001. <https://doi.org/10.1088/1361-6463/ab16b5>.
- Li, Y., Lee, C., Chen, R., Zhou, Q., and Shung, K.K. (2014). A feasibility study of *in vivo* applications of single beam acoustic tweezers. *Appl. Phys. Lett.* 105, 173701. <https://doi.org/10.1063/1.4900716>.
- Lam, K.H., Li, Y., Li, Y., Lim, H.G., Zhou, Q., and Shung, K.K. (2016). Multifunctional single beam acoustic tweezer for non-invasive cell/organism manipulation and tissue imaging. *Sci. Rep.* 6, 37554. <https://doi.org/10.1038/srep37554>.
- Youn, S., Choi, J.W., Lee, J.S., Kim, J., Yang, I.-H., Chang, J.H., Kim, H.C., and Hwang, J.Y. (2019). Acoustic Trapping Technique for Studying Calcium Response of a Suspended Breast Cancer Cell: Determination of Its Invasion Potentials. *IEEE Trans. Ultrason. Ferroelectrics Freq. Control* 66, 737–746. <https://doi.org/10.1109/TUFFC.2019.2894662>.
- Menz, M.D., Ye, P., Firouzi, K., Nikoozadeh, A., Pauly, K.B., Khuri-Yakub, P., and Baccus, S.A. (2019). Radiation Force as a Physical Mechanism for Ultrasonic Neurostimulation of the Ex Vivo Retina. *J. Neurosci.* 39, 6251–6264. <https://doi.org/10.1523/JNEUROSCI.2394-18.2019>.
- Li, Z., Wang, D., Fei, C., Qiu, Z., Hou, C., Wu, R., Li, D., Zhang, Q., Chen, D., Chen, Z., et al. (2021). The forbidden band and size selectivity of acoustic radiation force trapping. *iScience* 24, 101988. <https://doi.org/10.1016/j.isci.2020.101988>.
- Gong, Z., and Baudoin, M. (2022). Single Beam Acoustical Tweezers Based on Focused Beams: A Numerical Analysis of Two-Dimensional and Three-Dimensional Trapping Capabilities. *Phys. Rev. Appl.* 18, 044033. <https://doi.org/10.1103/PhysRevApplied.18.044033>.
- Lee, J., Teh, S.Y., Lee, A., Kim, H.H., Lee, C., and Shung, K.K. (2009). Single beam acoustic trapping. *Appl. Phys. Lett.* 95, 73701–73724. <https://doi.org/10.1063/1.3206910>.
- Chen, X., Lam, K.H., Chen, R., Chen, Z., Yu, P., Chen, Z., Shung, K.K., and Zhou, Q. (2017). An adjustable multi-scale single beam acoustic tweezers based on ultrahigh frequency ultrasonic transducer. *Biotechnol. Bioeng.* 114, 2637–2647. <https://doi.org/10.1002/bit.26365>.
- Lim, H.G., Lee, O.-J., Shung, K.K., Kim, J.-T., and Kim, H.H. (2020). Classification of Breast Cancer Cells Using the Integration of High-Frequency Single-Beam Acoustic Tweezers and Convolutional Neural Networks. *Cancers* 12, 1212. <https://doi.org/10.3390/cancers12051212>.
- Lim, H.G., Liu, H.-C., Yoon, C.W., Jung, H., Kim, M.G., Yoon, C., Kim, H.H., and Shung, K.K. (2020). Investigation of cell mechanics using single-beam acoustic tweezers as a versatile tool for the diagnosis and treatment of highly invasive breast cancer cell lines: an *in vitro* study. *Microsyst. Nanoeng.* 6, 39. <https://doi.org/10.1038/s41378-020-0150-6>.
- Yoo, J., Kim, H., Kim, Y., Lim, H.G., and Kim, H.H. (2022). Collapse pressure measurement of single hollow glass microsphere using single-beam acoustic tweezer. *Ultrason. Sonochem.* 82, 105844. <https://doi.org/10.1016/j.ulsonch.2021.105844>.

36. Baudoin, M., Thomas, J.-L., Sahely, R.A., Gerbedoen, J.-C., Gong, Z., Sivery, A., Matar, O.B., Smagin, N., Favreau, P., and Vlandas, A. (2020). Spatially selective manipulation of cells with single-beam acoustical tweezers. *Nat. Commun.* *11*, 4244. <https://doi.org/10.1038/s41467-020-18000-y>.
37. Lim, H.G., and Shung, K.K. (2017). Quantification of Inter-Erythrocyte Forces with Ultra-High Frequency (410 MHz) Single Beam Acoustic Tweezer. *Ann. Biomed. Eng.* *45*, 2174–2183. <https://doi.org/10.1007/s10439-017-1863-z>.
38. Pereira-Veiga, T., Schneegans, S., Pantel, K., and Wikman, H. (2022). Circulating tumor cell-blood cell crosstalk: Biology and clinical relevance. *Cell Rep.* *40*, 111298. <https://doi.org/10.1016/j.celrep.2022.111298>.
39. Suo, Y., Gu, Z., and Wei, X. (2020). Advances of In Vivo Flow Cytometry on Cancer Studies. *Cytometry A.* *97*, 15–23. <https://doi.org/10.1002/cyto.a.23851>.
40. Tan, Y., Sun, D., Wang, J., and Huang, W. (2010). Mechanical characterization of human red blood cells under different osmotic conditions by robotic manipulation with optical tweezers. *IEEE Trans. Biomed. Eng.* *57*, 1816–1825. <https://doi.org/10.1109/TBME.2010.2042448>.
41. Lee, J., and Shung, K.K. (2006). Radiation forces exerted on arbitrarily located sphere by acoustic tweezer. *J. Acoust. Soc. Am.* *120*, 1084–1094. <https://doi.org/10.1121/1.2216899>.
42. Lee, J., Lee, C., Kim, H.H., Jakob, A., Lemor, R., Teh, S.-Y., Lee, A., and Shung, K.K. (2011). Targeted cell immobilization by ultrasound microbeam. *Biotechnol. Bioeng.* *108*, 1643–1650. <https://doi.org/10.1002/bit.23073>.
43. Kang, S.-T., and Yeh, C.-K. (2013). Trapping of a mie sphere by acoustic pulses: effects of pulse length. *IEEE Trans. Ultrason. Ferroelectrics Freq. Control* *60*, 1487–1497. <https://doi.org/10.1109/TUFFC.2013.2721>.
44. Jung, C.Y. (1971). Permeability of bimolecular membranes made from lipid extracts of human red cell ghosts to sugars. *J. Membr. Biol.* *5*, 200–214. <https://doi.org/10.1007/BF02107724>.
45. Kim, S., Qiu, F., Kim, S., Ghanbari, A., Moon, C., Zhang, L., Nelson, B.J., and Choi, H. (2013). Fabrication and Characterization of Magnetic Microrobots for Three-Dimensional Cell Culture and Targeted Transportation. *Adv. Mater.* *25*, 5863–5868. <https://doi.org/10.1002/adma.201301484>.
46. Schwab, F.D., Scheidmann, M.C., Ozimski, L.L., Kling, A., Armbrrecht, L., Ryser, T., Krol, I., Strittmatter, K., Nguyen-Sträuli, B.D., Jacob, F., et al. (2022). MyCTC chip: microfluidic-based drug screen with patient-derived tumour cells from liquid biopsies. *Microsyst. Nanoeng.* *8*, 130. <https://doi.org/10.1038/s41378-022-00467-y>.
47. Shields, C.W., 4th, Reyes, C.D., and López, G.P. (2015). Microfluidic cell sorting: a review of the advances in the separation of cells from debulking to rare cell isolation. *Lab Chip* *15*, 1230–1249. <https://doi.org/10.1039/C4LC01246A>.
48. Zajac, M., Kotyńska, J., Worobiczuk, M., Breczko, J., and Naumowicz, M. (2022). The Effect of Submicron Polystyrene on the Electrokinetic Potential of Cell Membranes of Red Blood Cells and Platelets. *Membranes* *12*, 366. <https://doi.org/10.3390/membranes12040366>.
49. Zhu, R., Avsievich, T., Popov, A., and Meglinski, I. (2020). Optical Tweezers in Studies of Red Blood Cells. *Cells* *9*, 545. <https://doi.org/10.3390/cells9030545>.
50. Choi, H.K., Kim, H.G., Shon, M.J., and Yoon, T.Y. (2022). High-Resolution Single-Molecule Magnetic Tweezers. *Annu. Rev. Biochem.* *91*, 33–59. <https://doi.org/10.1146/annurev-biochem-032620-104637>.
51. Huang, L., Chen, Y., and Zhou, J. (2022). Interrogation of single-cell communications on microfluidic platforms. *Cell Rep. Phys. Sci.* *3*, 101129. <https://doi.org/10.1016/j.xcrp.2022.101129>.
52. Li, J., Wang, S., Wang, N., Zheng, Y., Yang, B., Wang, X., Zhang, J., Pan, B., and Wang, Z. (2021). Three dimensional acoustic tweezers with vortex streaming. *Commun. Phys.* *19*, 113. <https://doi.org/10.1038/s42005-021-00617-0>.
53. Gong, Z., and Baudoin, M. (2021). Three-Dimensional Trapping and Dynamic Axial Manipulation with Frequency-Tuned Spiraling Acoustical Tweezers: A Theoretical Study. *Phys. Rev. Appl.* *16*, 024034. <https://doi.org/10.1103/PhysRevApplied.16.024034>.
54. Ma, T., Yang, Y., Zhang, Q., Huang, J., Hu, Q., Li, Y., Wang, C., Zheng, H., and Zheng, H. (2022). 3D Acoustic Manipulation of Living Cells and Organisms Based on 2D Array. *IEEE Trans. Biomed. Eng.* *69*, 2342–2352. <https://doi.org/10.1109/TBME.2022.3142774>.
55. Gor'kov, L. (1962). On the forces acting on a small particle in an acoustical field in an ideal fluid. *Sov. Phys. Dokl.* *6*.
56. Mohanty, S., Fidler, R.J., Matos, P.M., Heunis, C.M., Kaya, M., Blanken, N., and Misra, S. (2022). SonoTweezer: An Acoustically Powered End-Effector for Underwater Micromanipulation. *IEEE Trans. Ultrason. Ferroelectrics Freq. Control* *69*, 988–997. <https://doi.org/10.1109/TUFFC.2022.3140745>.
57. Dholakia, K., Drinkwater, B.W., and Ritsch-Marte, M. (2020). Comparing acoustic and optical forces for biomedical research. *Nat. Rev. Phys.* *2*, 480–491. <https://doi.org/10.1038/s42254-020-0215-3>.

STAR★METHODS

KEY RESOURCES TABLE

REAGENT or RESOURCE	SOURCE	IDENTIFIER
Biological samples		
Human red blood cell	This paper	N/A
Deposited data		
Datasets and original code	Zenodo	https://doi.org/10.5281/zenodo.8349080
Software and algorithms		
Imaging software	Molecular Devices	MetaMorph
ImageJ	NIH	https://imagej.nih.gov
GraphPad Prism 9	GraphPad Software	https://graphpad.com
MATLAB R2020a	MATLAB R2020a	https://mathworks.com
Other		
Polystyrene	Polysciences	Polybead® microspheres
Hydrophone	Precision Acoustics	NH0040
Beam profile test system	IMP Systems	IPB760
Linear motor	Sigma Koki	OSMS20-85
Function generator	Stanford Research Systems	SG382
Power amplifier	Electronics & Innovation	525LA
Pulse-receiver	Imaginant Inc.	DPR500
Oscilloscope	Tektronix	DPO3032
Inverted microscope	Olympus	IX-73
CMOS camera	Hamamatsu Photonics	ORCA-Flash4.0 V3

RESOURCE AVAILABILITY

Lead contact

Further information and requests for resources should be directed to and will be fulfilled by the Lead Contact, Hyung Ham Kim (david.kim@postech.ac.kr).

Materials availability

This study did not generate new unique materials.

Data and code availability

- All datasets have been deposited at Zenodo and are publicly available as of the date of publication. DOIs are listed in the [key resources table](#).
- All original code has been deposited at Zenodo and is publicly available as of the date of publication. DOIs are listed in the [key resources table](#).
- Any additional information required to reanalyze the data reported in this paper is available from the [lead contact](#) upon request.

EXPERIMENTAL MODEL AND STUDY PARTICIPANT DETAILS

Human RBC

We directly extracted and utilized human blood obtained from individuals. Following sterilization of the donor's fingertip, 10 μ L of human blood was extracted utilizing a lancet. This blood was subsequently diluted, allowing us to obtain RBCs. We collected blood from a healthy volunteer, who had not undergone any previous testing. We utilized anonymized human blood, using it immediately without storage or culturing. After use, it was promptly discarded, and no genetic or personally identifiable information was collected. All procedures for preparing and measuring human blood samples in this study were approved by the Institutional Review Board (IRB) of POSTECH (PIRB-2022-R023).

METHOD DETAILS

Derivation of acoustic radiation force

Suppose that an incoming sound beam enters a sphere, and its pressure has a Gaussian distribution (P_s), as given by Equations 5 and 6.

$$P_s = p_0 \exp \left\{ - \frac{(x^2 + y^2)}{w(z)^2} \right\} \quad (\text{Equation 5})$$

$$w(z) = w_0 \sqrt{1 + \left(\frac{\lambda z}{\pi w_0^2} \right)^2} \quad (\text{Equation 6})$$

$w(z)$ and w_0 are the beam widths at the axial points z and $z = 0$. λ is the wavelength of the incident beam. The force potential U in an arbitrary pressure field was derived by Gor'kov and adopted to evaluate its trapping characteristics.⁵⁵ For a compressible sphere surrounded by an inviscid fluid of density ρ_0 , the potential U is expressed using Equations 7, 8, and 9.

$$U = 2\pi r^3 \rho_0 \left(\frac{\overline{P_s^2}}{3\rho_0^2 c_0^2} f_1 - \frac{\overline{v_s^2}}{2} f_2 \right) \quad (\text{Equation 7})$$

$$f_1 = 1 - \frac{\rho_0 c_0^2}{\rho c^2} \quad (\text{Equation 8})$$

$$f_2 = \frac{2(\rho - \rho_0)}{2\rho + \rho_0} \quad (\text{Equation 9})$$

c and c_0 are the speed of sound in the sphere and fluid, respectively. ρ and r are the density and radius of the sphere, respectively. P_s and v_s represent the pressure and particle velocity, respectively, at the position of the sphere. $\overline{(\)}$ denotes the temporal average of an argument. f_1 and f_2 are dimensionless factors that depend on the material properties of the fluid and the sphere, respectively. According to the linear Euler Equation 10 and its time-averaged term (7), Equation 11 can be further simplified to Equation 12.⁵⁶

$$\nabla P_s = -\rho_0 \frac{\partial v_s}{\partial t} \quad (\text{Equation 10})$$

$$\overline{v_s^2} = \frac{1}{2\rho_0^2 \omega^2} |\nabla P_s|^2 \quad (\text{Equation 11})$$

$$U = 2\pi r^3 \rho_0 \left(\frac{f_1}{3\rho_0^2 c_0^2} |P_s|^2 - \frac{f_2}{4\rho_0^2 \omega^2} |\nabla P_s|^2 \right) \quad (\text{Equation 12})$$

Consequently, the acoustic radiation force F acting on the sphere is equal to the negative gradient of U as follows:

$$F = -\nabla U = \frac{2\pi r^3}{\rho_0} \nabla \left(\frac{f_2}{4\omega^2} |\nabla P_s|^2 - \frac{f_1}{3c_0^2} |P_s|^2 \right) \quad (\text{Equation 13})$$

The PS bead and RBC trapping forces were calculated based on the derived equations. When acoustic pressure is applied to the bottom of the Petri dish with a Gaussian distribution, potential energy is generated by the pressure (Figure 1A). This energy created a trapping force that moved the PS bead and RBC in the Petri dish toward the focus of the ultrasound microbeam.

Single-element acoustic tweezers fabrication

For non-invasive cell trapping, a frequency range capable of generating trapping forces in the sub-pN range and enabling penetration up to several centimeters is required.⁵⁷ Based on numerical simulations, we observed that trapping forces of several pN were achieved with frequencies of 30 MHz and above (Figure S6A). A low frequency and a high f-number are desired to achieve deep penetration depth. Therefore, the appropriate frequency and f-number were chosen as 30 MHz and 4, respectively. Lithium niobate was used as the piezoelectric material for the tweezers, and the acoustic beam was focused using a mechanical press-focusing method. In the impulse response, the -6-dB center frequency was measured to be 34 MHz, and the bandwidth was measured to be 42% (Figure S1A). The acoustic pressure characteristics relative to the applied voltage were obtained using a hydrophone (NH0040, Precision Acoustics, Dorchester, UK) and beam profile test system (IPB760, IMP Systems, Gyeongsangbuk-do, South Korea) (Figure S1B). The lateral and axial beam widths were measured to be 0.256 and 5.9 mm, respectively (Figures S1C and S1D). The detailed acoustic properties of the fabricated tweezers are illustrated in Figure S1.

Trapping of the PS bead and RBC

Each PS bead and RBC sample was prepared by filling a Petri dish with 5 mL of HBSS and adding 1 μ L of PS beads (Polybead® microspheres, Polysciences, Inc., PA, USA) or blood collected using lancets. To prevent hemolysis of RBCs, HBSS was employed, and the cell trapping approach can be applied in other media types, such as plasma (Figure S6B). In all experiments of this study, 5- μ m PS beads, similar in size to RBCs, were used. For simulations, a size of 5 μ m was specified for all cases except for Figure S2, where the size was explicitly mentioned. Leaving RBCs in the dish for a long time (more than 1 hour) causes them to adhere to the bottom, obstructing trapping. To address this, we allowed approximately 5 minutes for RBCs to settle before trapping what did not adhere to the bottom. For cell sorting experiments, 1 μ L of PS beads and blood were placed together in a Petri dish. After the microparticles settled to the bottom, the tweezers were immersed in the sample and connected to the tweezers system (Figure S7). The tweezers were mounted on a 3-axis linear motor (OSMS20-85, Sigma Koki Co., Ltd, Tokyo, Japan). The applied signal was generated using a function generator (SG382, Stanford Research Systems, CA, USA) and amplified using a power amplifier (525LA, Electronics & Innovation, Ltd., NY, USA) with an output power of 25W. The applied signal is a square pulsed wave with a pulse repetition frequency (PRF) of 1 kHz and is amplified by 50 dB. The travel distance was measured from the pulse-echo signal using a pulser-receiver (DPR500, C, NY, USA) and an oscilloscope (DPO3032, Tektronix, OR, USA). After appropriately adjusting the distance between the microparticles and the focal point of the tweezers, an input signal was applied to generate the desired acoustic microbeam and trap the PS bead and RBC. In Figures 2, 3, and 4, the travel distance for PS beads was set at 12.4 mm, which was 250 μ m shorter than the focal depth, while for RBCs, the travel distance was set at 12.65 mm, which was equal to the focal depth.

Imaging setup and data analysis

The movement of the microparticles was observed using an inverted microscope (IX-73, Olympus, PA, USA) and recorded using a CMOS camera (ORCA-Flash4.0 V3, Hamamatsu Photonics, Shizuoka, Japan). If the time interval of the recorded video is too short, an error occurs in the shutter opening/closing time, which may affect the speed measurement. Therefore, a sufficiently long period of 0.5 s was used. Imaging software (MetaMorph, Molecular Devices LLC, CA, USA) enabled real-time microparticle imaging and distance measurements. The acquired images were processed using ImageJ (NIH, MD, USA), including mIP imaging and distance measurement through coordinates. Statistical analyses were performed using GraphPad Prism 9 (GraphPad Software, Inc., CA, USA), and graphical visualizations were performed using ImageJ, GraphPad Prism 9, and MATLAB R2020a (MathWorks, MA, USA).

Average velocity calculation

To directly evaluate the pattern of the trapping force, instantaneous acceleration is required; however, this is difficult to measure. In this study, the average velocity was used to analyze the force profile. Although the absolute values of the simulations and measurements cannot be compared, the behavior of the forces over distances can be evaluated indirectly. We calibrated the length of the number of pixels in the imaging software to measure the actual distance in the ImageJ coordinates. In the recorded microparticle movement, the number of frames indicates the movement's duration. Using the center point coordinates of each microparticle at the start and end frames, we measured the distance traveled. The average speed was calculated by dividing the distance by the travel time. In addition, we determined the distance from the focal point in the section where the average speed was measured.

QUANTIFICATION AND STATISTICAL ANALYSIS

All experiments discussed in this study were performed with at least three replicates, and data were presented as mean and standard deviation. Statistical details can be found in the legend of each figure.